Journal of Colloid and Interface Science 650 (2023) 1659–1670

Contents lists available at ScienceDirect

Journal of Colloid And Interface Science

journal homepage: www.elsevier.com/locate/jcis

# Liposomal aggregates sustain the release of rapamycin and protect cartilage from friction

Gregor Bordon [a], Shivaprakash N. Ramakrishna [b], Sam G. Edalat [c], Remo Eugster [a], Andrea Arcifa [d], Martina Vermathen [a], Simone Aleandri [a], Mojca Frank Bertoncelj [e], Julien Furrer [a], Peter Vermathen [f], Lucio Isa [b], Rowena Crockett [d], Oliver Distler [c], Paola Luciani [a,*]

[a] Department of Chemistry, Biochemistry and Pharmaceutical Sciences, University of Bern, Freiestrasse 3, 3012 Bern, Switzerland
[b] Laboratory for Soft Materials and Interfaces, Department of Materials, ETH Zurich, Vladimir- Prelog-Weg 1-5/10, 8093 Zurich, Switzerland
[c] Center of Experimental Rheumatology, Department of Rheumatology, University Hospital Zurich, University of Zurich, Wagistrasse 14, 8952 Schlieren, Switzerland
[d] Laboratory for Surface Science and Coating Technologies, EMPA, Uberlandstrasse 129, 8600 Dubendorf, Switzerland
[e] BioMed X Institute, Im Neuenheimer Feld 515, 69120 Heidelberg, Germany
[f] Magnetic Resonance Methodology, Institute of Diagnostic and Interventional Neuroradiology, University & Inselspital Bern, sitem-insel AG, Freiburgstrasse 3, 3010 Bern, Switzerland

## GRAPHICAL ABSTRACT

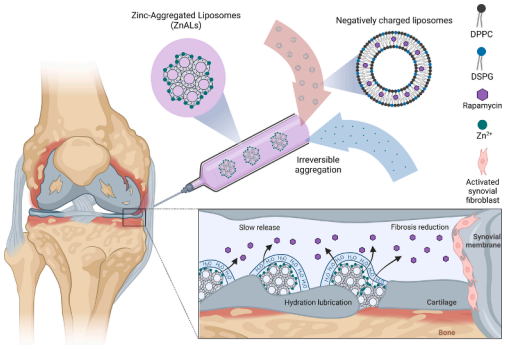


## ARTICLE INFO

*Keywords:*
Rapamycin
Liposomal aggregates
Sustained release
Aggregation kinetics
Liposomal morphology
Synovial fibroblasts
Osteoarthritis
Cartilage lubrication

## ABSTRACT

Liposomes show promise as biolubricants for damaged cartilage, but their small size results in low joint and cartilage retention. We developed a zinc ion-based liposomal drug delivery system for local osteoarthritis therapy, focusing on sustained release and tribological protection from phospholipid lubrication properties. Our strategy involved inducing aggregation of negatively charged liposomes with zinc ions to extend rapamycin (RAPA) release and improve cartilage lubrication. Liposomal aggregation occurred within 10 min and was irreversible, facilitating excess cation removal. The aggregates extended RAPA release beyond free liposomes and displayed irregular morphology influenced by RAPA. At nearly 100 μm, the aggregates were large enough to exceed the previously reported size threshold for increased joint retention. Tribological assessment on silicon

* Corresponding author.
*E-mail address:* paola.luciani@unibe.ch (P. Luciani).

https://doi.org/10.1016/j.jcis.2023.07.087
Received 30 March 2023; Received in revised form 7 July 2023; Accepted 13 July 2023
Available online 16 July 2023

surfaces and ex vivo porcine cartilage revealed the system's excellent protective ability against friction at both nano- and macro-scales. Moreover, RAPA was shown to attenuate the fibrotic response in human OA synovial fibroblasts. Our findings suggest the zinc ion-based liposomal drug delivery system has potential to enhance OA therapy through extended release and cartilage tribological protection, while also illustrating the impact of a hydrophobic drug like RAPA on liposome aggregation and morphology.

## 1. Introduction

Osteoarthritis (OA) is a debilitating chronic joint disease characterised by the degradation of articular cartilage, synovial fibrosis, and low-grade inflammation. It affects 7% of the global population, where women are disproportionately affected by the condition. The current treatment possibilities are very limited, relying primarily on non-steroidal anti-inflammatory drugs and analgesics, and joint replacement. For patients unresponsive to these medications, hyaluronic acid (HA) and glucocorticoids are prescribed, however, their use remains controversial. Several cellular therapies are becoming increasingly available, but they lack consistency of protocols or/and strong clinical data [1–3]. Overall, better treatments for OA remain a strongly unmet clinical need.

Rapamycin (RAPA) is an immunosuppressive drug that was first approved for the prevention of rejection in renal transplant recipients [4] and has been since tested for treatment of cancer [5], inflammatory diseases [6–8], and increasing longevity [9,10]. Recently, RAPA showed promise in OA therapy, as it reduces excessive chondrocyte apoptosis and inflammation, protecting the cartilage from further degradation [11,12]. Several *in vivo* studies have confirmed these effects, demonstrating that RAPA significantly reduces OA severity and damage to the articular cartilage [13–15]. The latest evidence shows that OA also perturbs the function of synovial fibroblasts (SFs) in the joint synovial membrane. SFs significantly contribute to cartilage damage in OA, and synovial fibrosis is associated with chronic joint pain [2,16,17]. While research on RAPA's effects on SF inflammation and senescence is gathering momentum [18–20], little is known about its impact on fibrotic OA SFs (OASFs). Additionally, the systemic use of RAPA is hindered by its adverse effects, but a growing body of literature suggests that local intraarticular injection is a promising avenue for OA treatment [13,14].

Previous research has proposed that a combination of pharmacological intervention and cartilage lubrication would yield a synergistically improved treatment for OA, but there are still no therapies available for patients exerting this dual activity [21,22]. Early investigations demonstrated that phospholipid-based liposomes, namely small unilamellar vesicles (SUVs), can improve boundary lubrication and wear of cartilage through hydration of the phospholipid headgroups [23–26]. More recently, scientists developed a liposomal system that sustained the drug release of D-glucosamine sulfate for OA treatment and succeeded in improving the lubrication [22]. Although liposomes show great promise for OA treatment from the standpoint of biocompatibility, boundary lubrication, and controlled drug release, typical SUVs suffer from several drawbacks. Small SUVs can penetrate deep into cartilage, and when tested on ex vivo cartilage models, they exhibit worse lubrication properties compared to larger phospholipid-based vesicles that can be retained closer to the tissue's surface [27]. Furthermore, a small particle size of below 300 nm was correlated with rapid clearance from the joint, which calls for frequent administration of the formulation and an increased risk of inducing infection [28,29]. In comparison, particles above 10 μm can avoid phagocytosis by macrophages and can be retained in naïve as well as in the inflamed joints for over 6 weeks [29–31]. For these reasons, the utility of small phospholipid-based particles, such as SUVs is in practice limited and the development of new drug delivery systems with larger particle size and ability to sustain the drug release is imperative for better treatment of OA. Our group previously reported the ability of calcium and magnesium cations to aggregate the negatively charged liposomes into larger aggregated liposomes (ALs) forming injectable depots [32] and the resulting slower release of bupivacaine *in vitro* [33]. *In vivo* results suggested that the aggregates also increased the drug's area under the curve in plasma compared to the non-depot system and modulated the particle clearance from the injection site. Here, we tested zinc, a divalent cation known for its anti-inflammatory and antioxidant effects [34–36], as an alternative to the aforementioned aggregating agents. Our results demonstrate that aggregating negatively charged liposomes with 150 mM zinc produces irreversible ALs (ZnALs) with a diameter exceeding 90 μm, which has been shown to significantly increase the retention time in synovial joints. [29,31]. The irreversible nature of the particles is not significant only from a pharmacokinetic perspective, but also technological, because it allows downstream processing, such as purification from excess zinc prior to administration. We further characterised the aggregation properties of the system in depth and showed that ZnALs are able to improve lubrication through testing with lateral force microscopy (LFM) as well as sustain the release of RAPA with 86 % of the drug released after 7 days. These findings suggest that the system has potential for the dual treatment of OA through maintaining a low level of friction in the joint and sustaining the release of RAPA, which can decrease fibrotic markers in OASFs.

## 2. Materials and methods

### 2.1. Materials

The phospholipids 1,2-dipalmitoyl-*sn-glycero*-3-phosphocholine (DPPC) and 1,2-distearoyl-*sn-glycero*-3-phospho-(10-*rac*-glycerol) sodium salt (DSPG) were kindly gifted by Lipoid (Ludwigshafen, Germany). Rapamycin (sirolimus) was obtained from R&S Pharmchem (Pudong Districts, Shanghai, China). Zinc chloride (98 % purity, reagent grade), ketoconazole (99–101 % purity), and cholesterol (≥99 % purity) were purchased from Sigma-Aldrich-Merck (St Louis, MO, USA). Trifluoroacetic acid and 1 M HEPES solution were obtained from Carl Roth (Karlsruhe, Germany). 1,1′-dioctadecyl-3,3,3′,3′-tetramethylindodicarbocyanine, 4-chlorobenzenesulfonate salt (DiD, catalog number: D7757) was purchased from Thermo Fisher Scientific (Waltham, MA, USA). Chloroform and methanol were obtained from Fisher Scientific (Schwerte, Germany). All chemicals were used as received. Ultrapure water of resistivity 18.2 MΩ.cm was produced by a Barnstead Smart2 pure device from Thermo Scientific (Pittsburgh, USA). Porcine knee cartilage was obtained from a local slaughterhouse in Münchenbuchsee, Switzerland. The deuterated solvents $D_2O$ 99.9 % and $CDCl_3$ 99.8 % were obtained from Deutero GmbH and Eurisotop, respectively. Phosphate buffered saline (PBS) was prepared from mixing adequate amounts of 50 mM $K_2HPO_4$ and 50 mM $NaH_2PO_4$ solutions in $D_2O$ containing 0.9 % NaCl. The pH was adjusted to 7.3.

### 2.2. Preparation and characterisation of liposomes

Liposomes with 25 mol% DSPG and varying DPPC/cholesterol content were prepared with thin-film hydration method. Lipid stock solutions in a chloroform/MeOH mixture (75/25 v/v) were dried under nitrogen flow and kept under vacuum overnight to remove residual solvents. Vesicles of 20 mM final lipid concentration were formed by hydration with 20 mM HEPES buffer at pH 7.4, heating to 70 °C, and mixing. The formed vesicles were freeze-thawed 6 times and

subsequently extruded 10 times through a 200 nm polycarbonate membrane (Sterlitech Corporation, USA) with a LIPEX extruder at 70 °C (Evonik, Canada). The mean hydrodynamic diameter and polydispersity index (PDI) were measured with dynamic light scattering (DLS) analyser Litesizer 500 (Anton Paar, Austria) at 25 °C with a backscatter angle of 175° and a 658 nm laser. The zeta potential was assessed with laser Doppler microelectrophoresis using the same instrument and Omega cuvette (Anton Paar, Austria). Liposome stability was evaluated for 16 weeks at 4 °C. Formulations were used within 24 h from extrusion for all testing.

### 2.3. Encapsulation efficiency of RAPA

RAPA was dissolved in MeOH and added to the lipid film in varying molar lipid: drug ratios, by keeping the lipid content constant. Encapsulation efficiency was calculated according to the formula below:

$$EE\% = \frac{amount\ of\ drug\ encapsulated}{total\ amount\ of\ drug} \times 100\%$$

The encapsulated RAPA was quantified after removal of unencapsulated RAPA with size exclusion chromatography (*SEC*) column (PD MidiTrap, G-25, Cytiva, USA) according to the manufacturer's protocol. The drug concentration in samples was measured with high-performance liquid chromatography (HPLC) using a reverse phase $C_{18}$ Nucleosil 100–5 (4.0 × 250 mm; 5.0 μm particle size, Macherey-Nagel, Germany) column and mobile phase consisting of MeOH/water (90/10 v/v) + 0.1 % trifluoroacetic acid at a flow rate of 1 mL/min, temperature 50° C and UV detection at λ = 278 nm. Ketoconazole was added to all samples as an internal standard at concentration of 0.2 mg/mL.

### 2.4. In vitro drug release

Release of RAPA from liposomes and ZnALs was tested *in vitro* using a custom-made dialysis device (**Figure S1**), with dimensions similar to a 2 mL Slide-A-Lyzer MINI (Thermo Scientific, USA) and a disposable polycarbonate membrane with 100 nm pore size (Figure S1). This design allowed us to accommodate a up to 50 mL of release medium and provided the flexibility to select the desired disposable polycarbonate membranes with 100 nm pore size (Figure S1), catering specifically to the requirements of our study. The release medium was composed of 10% EtOH in ultrapure water to maintain RAPA stability and achieve sink conditions, as rapamycin is sensitive to chemical degradation, particularly in the presence of higher salt concentrations, and requires an organic solvent to enhance its solubility [37,38]. To confirm the stability of liposomes during the release study, we monitored their size with dynamic light scattering (DLS) throughout the duration of the experiment, as shown in **Figure S2**. A volume of 1 mL of each sample was added into the dialysis device and 48 mL of the release medium were added to the acceptor chamber. The loaded dialysis devices were placed in the incubator at 37 °C while shaking at 10 rpm. Throughout the 7 days of the study's duration, the release medium from the acceptor chamber was aliquoted and fully replaced with a fresh one at each time point. The aliquots were frozen in liquid nitrogen and lyophilised. Each sample was resuspended with the internal standard solution and RAPA content was determined with HPLC.

### 2.5. Preparation and characterisation of ZnALs

Aggregated liposomes (ALs) were prepared through a four-time dilution of 20 mM liposomes with aqueous solutions containing different concentrations of $ZnCl_2$ ($Zn^{2+}$) and gentle stirring for 5 min. Keeping the volume ratios constant allowed for constant liposome and drug concentration in ZnALs at varying $Zn^{2+}$ concentrations. ALs were characterised via turbidimetric scattering measurements using a microplate reader, as previously reported [32]. Briefly, 50 μL of liposomes with an initial lipid concentration of 20 mM were mixed with 150 μL $Zn^{2+}$ solution in a quartz 96-well microtiter plate with a clear and flat bottom (Hellma GmbH & Co. KG, Germany). The mixture was gently mixed for 30 min, and the optical density was measured with an Infinite M Pro 200F-PlexNano microplate reader (Tecan, Switzerland) at 450 nm. The zeta potential of ZnALs was measured with the Litesizer 500 in the same manner as for the liposomes. Stability upon dilution was tested by diluting ALs 400 times with ultrapure water and subsequently performing a size measurement with the DLS at different time points. The presence and size of aggregates were determined with laser diffraction measurements, which were performed with PSA 1190 LD (Anton Paar GmbH, Austria) after 400x dilution in water as a dispersion medium where the obscuration parameter was set to 1–7 %. The optimization of input parameters such as stirring and pump speed was defined in order to obtain repeatable measurements. Stirring was set to slow (150 rpm) and the pump speed was put to medium setting (120 rpm). To further confirm the presence of aggregates upon 400x dilution, a nanoparticle tracking analysis (NTA) was performed using Zetaview (Particle Metrix, Germany) with a 488 nm laser, camera sensitivity of 58 and a 100 m/s shutter value. Aggregation kinetic experiments were performed with PSA using a series of 180 measurements with a measurement time of 10 s between each point. D50 was recorded and plotted over time, where 3 time points were averaged together as technical repeats to account for the measurement fluctuations. Prior to testing, the ZnALs underwent a purification process to eliminate excess $Zn^{2+}$. This was achieved through a 4 h dialysis in 0.5 L of ultrapure water, utilizing Float-A-Lyzers G2, 8–10 kDa MWCO (LubioScience GmbH, Switzerland), and hourly complete replacement of medium. $Zn^{2+}$ concentration was measured using inductively coupled plasma mass spectrometry (ICP-MS, NexION 2000, PerkinElmer, USA). Calibration standards, internal standards, and samples were prepared using a 2 % (w/w) $HNO_3$ solution (BASF SE, Germany) as the matrix. During measurements, a 10 μg/L yttrium solution was utilized as the internal standard during measurements. The ICP-MS system was calibrated with standards (TraceCERT Merck, Germany) ranging from 1 to 500 μg/L $Zn^{2+}$.

### 2.6. Differential scanning calorimetry (DSC)

Interactions between the phospholipid bilayer and RAPA were examined with a DSC 250 (TA Instruments, USA). Multilamellar liposomes and ZnALs (150 mM $Zn^{2+}$) with or without RAPA were prepared in a final concentration of 20 mM and 12 μL were transferred in a Tzero® aluminum pan and hermetically sealed. A volume of 12 μL of 20 mM HEPES was used as a reference. Samples were pre-heated to 60 °C, kept at that temperature for 5 min, and then cooled down to 10 °C. Next, two heating and cooling cycles were performed between 10 °C and 70 °C at the rate of 2 °C/min. The last cycle was used for the evaluation of the thermal profile and the calculation of hysteresis. The enthalpy values were normalized to the phospholipid amounts in the samples.

### 2.7. $^1H$ NMR spectroscopy

For the NMR experiments, liposome preparation and RAPA encapsulation were done as described in Sections 2.2 and 2.3 using $D_2O$-based PBS for hydration. In addition, RAPA was dissolved in $CDCl_3$ and used as reference. The liquid state NMR experiments on RAPA dissolved in $CDCl_3$ were performed on a Bruker Avance III HD spectrometer (Bruker BioSpin, Fällanden, Switzerland) operating at a resonance frequency of 400.13 MHz using a 5 mm BBFO SmartProbe with a z-gradient coil. The temperature was set to 300 K. 1H1H-NOESY spectra were acquired using the NOEsygpphpp sequence from the Bruker pulse program library. The number of scans was set to 16, the relaxation delay to 1 s, the spectral width in both dimensions (f2, f1) to 12 ppm, and the number of data points to 2 k and 128 in f2 and f1, respectively. A mixing time for NOE build-up of 500 ms was used.

The High Resolution Magic Angle Spinning (HR-MAS) NMR experiments on liposome/RAPA in PBS-$D_2O$ were performed on a Bruker

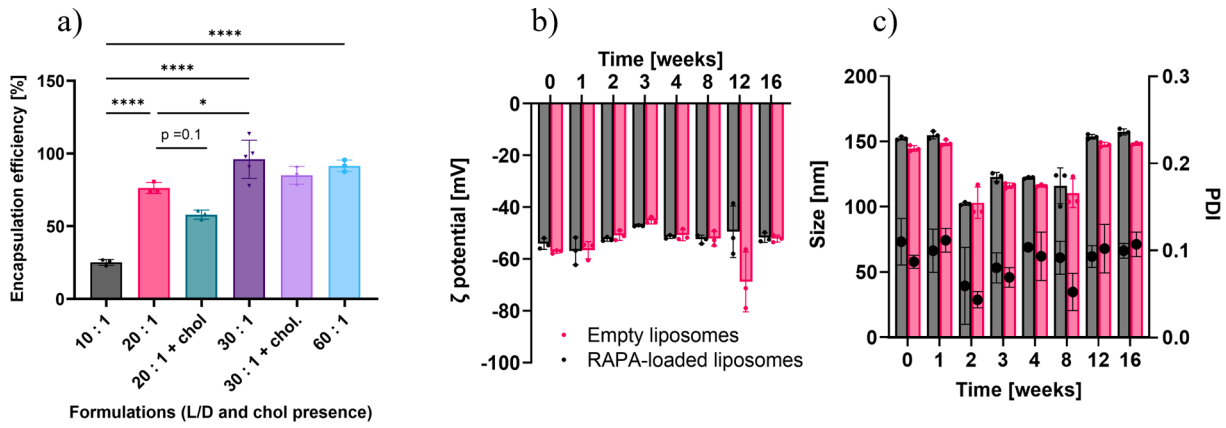


**Fig. 1.** a) EE% of RAPA in liposomes at different L/D. the formulations without chol had the composition DPPC:DSPG = 75:25 (mol:mol) and the formulations with chol DPPC:DSPG:chol = 45:25:30 (mol:mol:mol). b) Stability of zeta potential of the formulation with 30:1 (mol:mol) L/D without chol over 16 weeks. c) Stability of liposomes with 30:1 L/D without chol over 16 weeks with size on the left y-axis represented in bars and PDI on the right y-axis represented with the scatter plot. One-way ANOVA with Tukey's multiple comparisons test was run. Statistical significance is designated as: *P < 0.05 **P < 0.01, ***P < 0.001, ****P < 0.0001.

**Table 1**
Liposomes' properties at 30:1 (mol:mol) L/D, without chol.

| | Size [nm] | PDI | ζ-potential [mV] |
|---|---|---|---|
| Empty | 145 ± 2 | 0.11 ± 0.03 | −57.2 ± 0.6 |
| Loaded | 152 ± 1 | 0.087 ± 0.008 | −54.0 ± 2.0 |

Avance II spectrometer (Bruker BioSpin, Fällanden, Switzerland) operating at a resonance frequency of 500.13 MHz using a 4 mm HR-MAS dual inverse $^{1}H/^{13}C$ probe equipped with a z-gradient directed along the magic angle axis. The temperature was set to 333 K and the MAS rate to 8 kHz. The 1D 1H NMR spectrum was acquired using the zg sequence applying 256 scans, a relaxation delay of 4 s, a spectral width of 16 ppm and a data size of 32 k points. 1H1H-NOESY spectra were acquired using the NOEsyph sequence from the Bruker pulse program library. The number of scans was set to 128, the relaxation delay to 2 s, the spectral width in both dimensions (f2, f1) to 14 ppm, and the number of data points to 2 k and 256 in f2 and f1, respectively. A mixing time for NOE build-up of 100 ms was used.

All spectra were acquired and processed using the Bruker Topspin software versions 3.5 and 4.0.9, respectively.

### 2.8. Microscopic imaging of liposomes and ZnALs

Liposomes and ZnALs were imaged with fluorescence and cryogenic transmission electron microscopy (cryo-TEM) to assess the morphology. For fluorescence microscopy, lipid films for liposome preparation were stained with 0.05 mol% of the non-exchangeable lipophilic dye DiD. Liposomes and ZnALs were prepared as described above, while being protected from light. A volume of 20 µL of formulations was added on a slide and covered with a glass coverslip to be imaged with an inverted fluorescence microscope (Nikon Eclipse-Ti, Canada) through Tx red filter. For cryo-TEM, a volume of 6–8 µL of each sample was applied onto a gold grid covered by a holey gold film (UltrAuFoil 2/1, Quantifoil Micro Tools GmbH, Jena, Germany). Excess of liquid was blotted automatically between two strips of filter paper or only from the backside of the Grid. Subsequently, the samples were rapidly plunge-frozen in liquid ethane (cooled to 180 °C) in a Cryobox (Carl Zeiss NTS GmbH, Oberkochen, Germany). Excess ethane was removed with a piece of filter paper. The samples were transferred immediately with a Gatan 626 cryo-transfer holder (Gatan, Pleasanton, USA) into the pre-cooled Cryo-electron microscope (Philips CM 120, Eindhoven, Netherlands) operated at 120 kV and viewed under low dose conditions. The images were recorded with a 2 k CMOS Camera (F216, TVIPS, Gauting, Germany). In order to minimize the noise, four images were recorded and averaged to one image.

### 2.9. Cell culture

SFs were obtained from four consenting OA patients (according to ethics approvals BASEC-Nr. 2019–00674 and BASEC Nr. 2019–00115) and plated onto 25 $cm^2$ flasks and 6-well (clear, Corning, USA) or 96-well (black with clear bottom, Thermo Fisher Scientific, USA) plates following standard protocols [39]. Cells were cultured at 37 °C in a humidified atmosphere at 5 % $CO_2$ with Dulbecco's modified Eagle's medium (DMEM; Life Technologies) supplemented with 10 % fetal calf serum (FCS), 50 U $mL^{-1}$ penicillin/streptomycin, 2 mM L-glutamine, 10 mM HEPES, and 0.2 % amphotericin B (all from Life Technologies). OASFs were used for experiments between passages 4 and 6 when they reached confluency.

### 2.10. Toxicity of RAPA and ZnALs

OASFs were counted with Countess 3 FL (Thermo Fisher Scientific, USA) using trypan blue and seeded onto a 96-well plate at a density of 5′000 cells per well. After overnight incubation, the cells were treated with 200 µL of different conditions and incubated for 48 h. Upon incubation, the cells were stained with the LIVE/DEAD™ Viability/Cytotoxicity Assay Kit (Thermo Fisher Scientific, USA) according to the manufacturer's protocol. Briefly, the medium was aspirated, and the cells were washed with DPBS (Thermo Fisher Scientific, USA) before being stained with calcein and Sytox Deep Red dyes. Cells were incubated for 30 min at RT and washed with DPBS. The dead control was prepared by fixing the cells in ice-cold ethanol as per manufacturer's recommendations. Fluorescence was measured with a plate reader (BioTek Instruments, USA) in a bottom area scan mode with a 35 gain. Fluorescence intensity of alive cells was measured with a 528/20 nm filter after the excitation at 485 nm wavelength. Dead cells' fluorescence was excited at 530 nm and the emission was detected with 590/35 nm filter. Viability percentage was normalised to the fluorescence intensity of the untreated condition, which was treated with normal medium. Images were taken with a widefield fluorescence microscope (Zeiss AxioObserver Z1, Germany) using GFP (cyan) and DsRed (green) fluorescence filters.

### 2.11. Gene expression

For gene expression experiments, cells were seeded in the same way as described for the toxicity experiments above. The fibrotic response

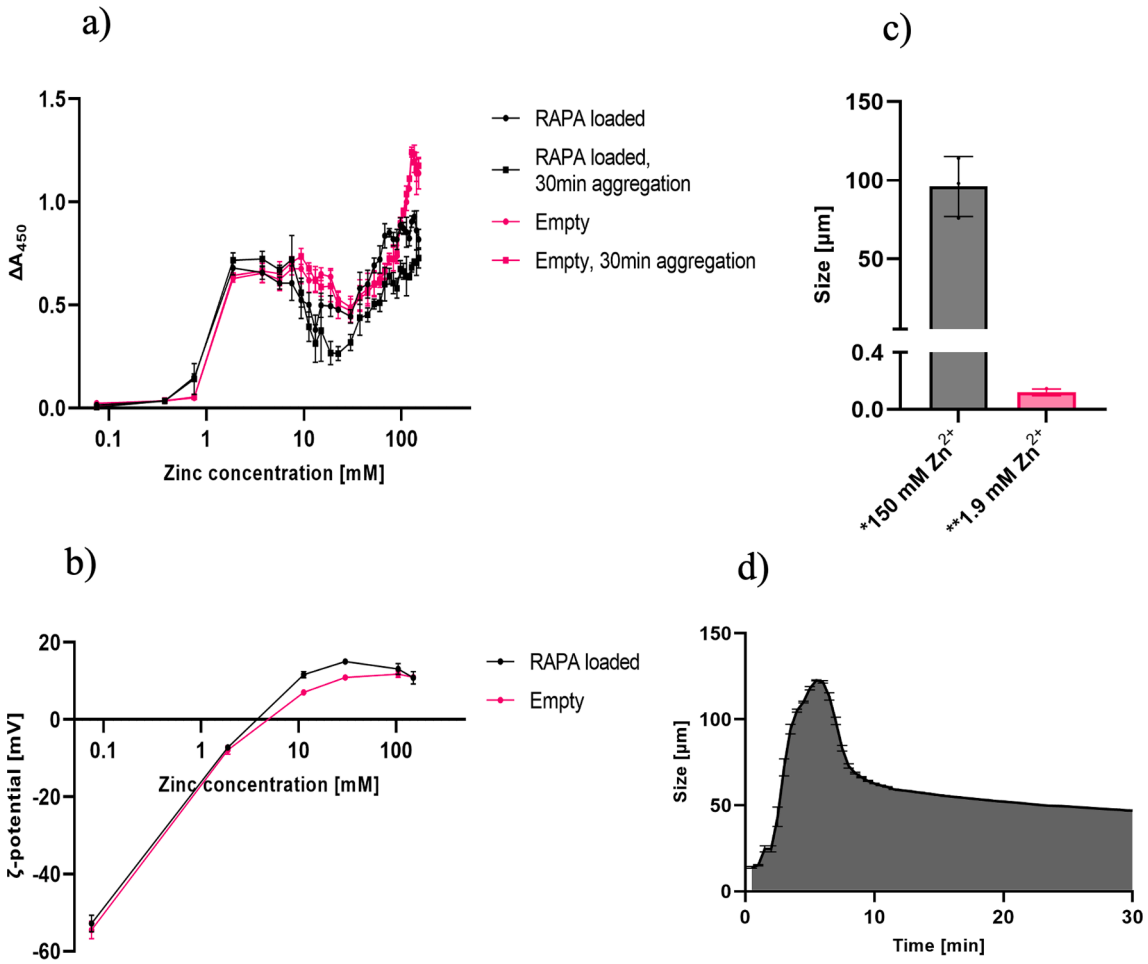


**Fig. 2.** a) ZnAls' aggregation profile measured at different $Zn^{2+}$ concentrations via a plate reader at 450 nm, immediately after mixing or after 30 min of gentle mixing. Final lipid concentration was 5 mM b) ζ.-potential of ZnALs at different $Zn^{2+}$ concentrations. c) Size after dilution with ultrapure water to a final $Zn^{2+}$ concentration below 0.5 mM. *Measured with PSA. **Measured with DLS. d) Aggregation kinetics of liposomes in 150 mM $Zn^{2+}$ measured with PSA – measurements were performed in 3 technical replicates at 30 s timepoints.

**Table 2**
DSC results of empty and RAPA-loaded MLVs and ZnALs (150 mM $Zn^{2+}$). The change in enthalpy was normalized to the mass of phospholipids in the samples, while the reported results represent the calculated mean values ± standard deviation of at least 3 replicates. Thermograms are available in Figure S4 in Supplementary Information.

| | $T_m$ [°C] | ΔH [J/g] | Peak width [°C] | T(pretr.) [°C] | ΔH(pretr.) [J/g] |
|---|---|---|---|---|---|
| Empty MLVs | 43.66 ± 0.03 | 35 ± 3 | 3.27 ± 0.03 | 36.0 ± 0.2 | 2.0 ± 0.4 |
| Loaded MLVs | 43.11 ± 0.02 | 33 ± 5 | 4.6 ± 0.2 | n.a. | n.a. |
| Empty ZnAL | 43.9 ± 0.1 | 1.0 ± 0.6 | 2.3 ± 0.2 | n.a. | n.a. |
| Loaded ZnAL | n.a. | n.a. | n.a. | n.a. | n.a. |

**Table 3**
Results of size measurements of ZnALs at different $Zn^{2+}$ concentrations with DLS and PSA reported as mean ± standard deviation of at least 3 replicates.

| [$Zn^{2+}$] in ZnALs | Size after dilution – DLS | Size after dilution – PSA |
|---|---|---|
| 1.9 mM | 119 nm ± 20 nm | Not measurable |
| 150 mM | Not measurable | 96 μm ± 19 μm |

was stimulated by adding 10 ng/mL of TGFβ to the medium together with the tested conditions. After 48 h incubation, cells were lysed, and RNA was extracted with a Quick-RNA Microprep Kit (Zymo Research, USA) as well as on-column DNase I digested according to the manufacturer's protocol. The purity and amount of RNA were determined by measuring the OD at a ratio of 260 to 280 nm with Nanodrop (Thermo Fisher Scientific). RNA was reverse transcribed and SYBRgreen real-time PCR was performed. Data were analysed with the comparative CT methods and presented as $2^{-\Delta\Delta CT}$ (i.e., x-fold) as described elsewhere [40] using RPLP0 as a housekeeping gene for sample normalization. Primer sequences are available in Supplementary Information.

### 2.12. Nanotribology

Nanotribology measurements were performed between silica probes sliding against silicon substrates by means of colloidal probe lateral force microscopy (CP-LFM) using a Bruker Dimension Icon AFM. Tipless Au-coated cantilevers (CSC-38, Mikromash, Bulgaria) were used for the measurments. Cantilever spring constants were determined using the thermal-noise method [41] for normal spring constants and Sader's method [42] for torsional spring constants. Approximately 8 μm diameter silica particles (EKA Chemicals AB, Kromasil R) were attached to the end of the tipless cantilever using two-component epoxy glue via a home-built micromanipulator. Four different colloidal probes were prepared and treated with UV/ozone for 30 min before the measurement. Four silicon wafers (~1x1 cm) were treated with UV/ozone and

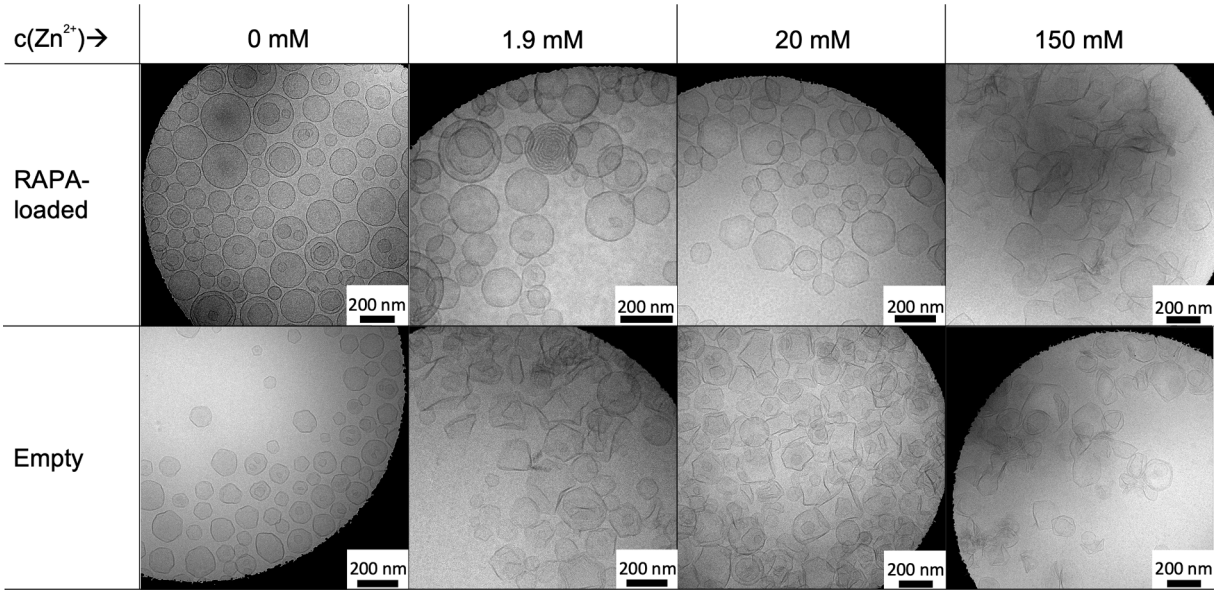


**Fig. 3.** Cryo-TEM images of empty and RAPA-loaded formulations with different $Zn^{2+}$ concentrations.

used as substrates. Prior to each measurement, the silicon substrates, but not the silica colloid probe, were immersed in either PBS, $Zn^{2+}$ solution, ZnAL, or liposome solutions (5 mM) for 30 min and rinsed with ultrapure water [22]. CP-LFM measurements were conducted in buffer solution, and friction loops were recorded by scanning the cantilever laterally over the surface. For each applied load, at least five friction loops were acquired, and the average friction values were obtained from trace and retrace curves. Coefficient of friction (COF) values were determined from the slope of the friction force vs normal force graphs. Lateral-force calibration was conducted using the "test-probe method" described by Cannara et al [43] by moving a test probe (a reference cantilever glued with a silica particle of diameter ~40 μm) laterally into contact with a silicon wafer (1x1 cm) used as a "hard wall" to obtain lateral sensitivity values.

### 2.13. Macrotribology

The macroscopic friction behaviour of cartilage sliding against cartilage in the presence of PBS, $Zn^{2+}$ solution, ZnALs, or liposome solutions was investigated with a UMT-2 tribometer (Bruker, USA) operating in linear reciprocating mode. The counterparts consisted of two portions of cartilage that were cut from porcine knee and stored at −20 °C until use. Cartilage was glued to the upper and lower surfaces of the tribometer shortly before testing. During each experiment, a load of 1 N was applied to the upper specimen (5x5 mm) and sliding took place over a 2 mm stroke length at a frequency of 1 Hz for 10 min. The specimens were completely immersed in the lubricant for the entire duration of the test. All tests were conducted at a constant temperature of 20 °C and a data acquisition frequency of 500 Hz. The representative coefficient of friction (COF) of each test was computed from the raw data of lateral and normal force as the average of each friction loop, taking only the central 90 % portion of each friction loop to avoid transients associated with the two ends of the stroke length. In addition, the first 20 % of the loops were excluded so that only the steady-state friction was processed, and the running-in phase was excluded.

### 2.14. Statistical analysis

All experiments were carried out in at least three replicates unless otherwise stated. The reported values are means with ±standard deviation. Microsoft Excel was used for general calculations, while GraphPad Prism 9.5 was used for plotting, performing the one-way ANOVA and Tukey's test.

## 3. Results & discussion

### 3.1. Preparation of liposomes and drug encapsulation

Drugs with low water solubility, such as RAPA, must be formulated to increase their bioavailability. Encapsulating them in liposomes is an effective way to solubilize the molecules, enhance their therapeutic index, and enable controlled release [21,44]. A key factor in liposome production is the encapsulation efficiency (EE%), with a low EE% requiring further purification to remove the unencapsulated drug, leading to increased production cost and complexity. The EE% is highly dependent on the drug's chemical properties, the composition of the liposomes, and the lipid-to-drug ratio (L/D) [45]. The impact of both was investigated in Fig. 1, where the higher L/D yielded higher EE%.

This is to be expected, as RAPA is highly hydrophobic and a greater amount of phospholipid gives more space for the drug to be encapsulated within the bilayer [46]. Chol is oftentimes added to the formulations to modulate the membrane properties such as thickness, packaging, and fluidity, which in turn can lead to decreased leakage of the drug from the liposomes [45]. On the other hand, the results illustrated in Fig. 1**a)** show that the presence of 30 mol% chol decreased the EE%. The highest EE% above 91 % was obtained with the L/D of 30:1 and 60:1 without chol and in order to keep a relevant therapeutic dose, the 30:1 formulation was used for all further experiments. These results are congruent with other studies, where RAPA [47] and other hydrophobic drugs were encapsulated in chol-containing liposomes [48]. The accepted explanation for this is that the addition of chol in the phospholipid bilayer reduces the size of hydrophobic cavities, which leaves less space for the encapsulation of lipophilic drugs, decreasing the drug-lipid interactions and hence, the EE% [46–49]. Table 1 demonstrates the difference in size between empty and RAPA-loaded liposomes, as measured by DLS in ultrapure water. The size of RAPA-loaded liposomes exhibited a slight but statistically significant increase compared to the empty liposomes, with a p-value $< 0.01$. Both systems displayed a low polydispersity index (PDI) of below 0.2, indicating a relatively uniform size distribution within the liposomal samples. Fig. 1**b)** and **c)** show that the liposomes were stable for a period of at least 16 weeks, with a slight decrease in size at week 2, which was already reported for DSPG/PC liposomes previously [32] and subsequent return to normal size at week 12.

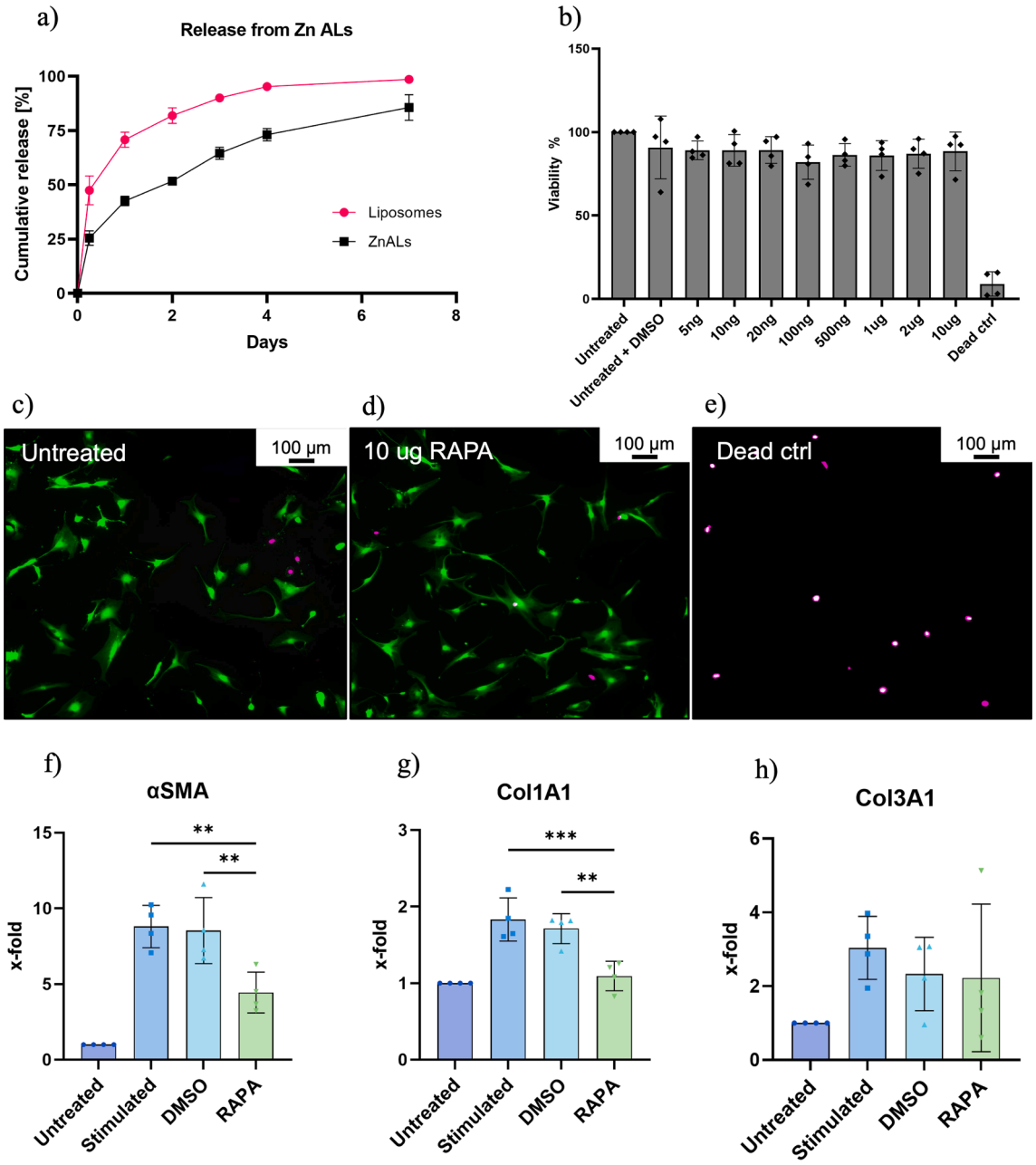


**Fig. 4.** a) Release of RAPA from liposomes and znals at 150 mM $Zn^{2+}$ in 10% EtOH. b) Toxicity of RAPA on human OASFs stained with calcein; fluorescence was measured with a plate reader. c) Fluorescence microscopy image of untreated OASFs after 48 h incubation and subsequent staining with calcein and SYTOX Deep Red. Live cells are coloured in green and dead in magenta. d) Cells at 10 µg/mL RAPA. e) Dead cells treated with 70% EtOH. f) Gene expression of αSMA, g) Col1A1, h) and Col3A1 in OASFs that were stimulated with TGFβ (10 ng/mL) and treated with RAPA (1 µg/mL) for 48 h. One-way ANOVA and Tukey's multiple comparisons test were run. Statistical significance is designated as: *P < 0.05 **P < 0.01, ***P < 0.001.

### *3.2. Fabrication and characterisation of zinc aggregated liposomes (ZnALs)*

Small particles like liposomes are rapidly cleared from synovium and therefore the administration of larger particles is preferable [29]. Cationic vehicles have been recently used to enhance interaction with negatively charged cartilage surface [50,51], but liposomes containing high amounts of positively charged phospholipids can elicit toxicity and inflammation [52,53]. To address this issue, we specifically selected zinc ion as the aggregating agent for our liposomal formulation, considering its reported anti-inflammatory properties and potential benefits in the context of osteoarthritis treatment. We developed a liposomal formulation with anionic phospholipids that aggregate upon the addition of $Zn^{2+}$, resulting in slightly positively charged ZnALs in the µm-range (Fig. 2**b), c)**).

The aggregation is propagated by the neutralization of negatively charged liposomes with $Zn^{2+}$, where the attractive van der Waals forces gain the upper hand. This is reflected in the secondary maximum on the aggregation profile on Fig. 2**a)**. After further addition of the cation, more $Zn^{2+}$ is bound on the surface of liposomes, which reverses the charge to +15 mV at 20 mM $Zn^{2+}$ content and stabilises smaller particles. This phenomenon is seen as the secondary minimum in Fig. 2**a)** and was previously observed in reports that focused on the coating of the anionic liposomes with polycations e.g., polylysine [54,55]. The continued introduction of $Zn^{2+}$ to the final concentration of 150 mM induces a global maximum in the profile, where a dip in the ζ-potential to 11 mV

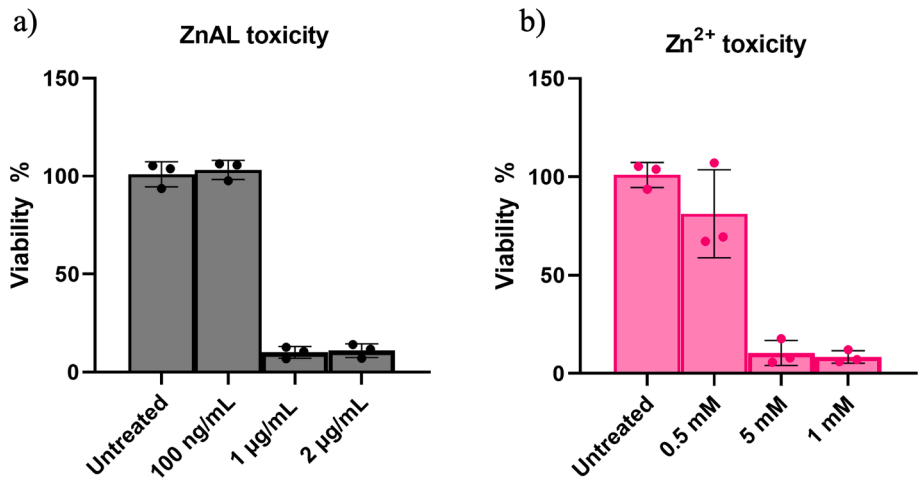


**Fig. 5.** a) Toxicity of purified ZnALs with RAPA doses 100 ng/mL, 1 µg/mL, and 2 µg/mL. b) Toxicity of free zinc ions in concentrations that are present in purified ZnALs at above RAPA doses (Table S1).

can be observed for both empty and RAPA-loaded systems. The two systems exhibit distinct differences, with the former showing a less pronounced minimum at 20 mM $Zn^{2+}$. This is likely due to a lower increase of ζ-potential at 20 mM $Zn^{2+}$ for the empty system, reaching only +11 mV compared to +15 mV for loaded ZnALs. The lower ζ-potential results in weaker electrostatic repulsion, promoting the formation of larger particles due to enhanced aggregation. These shifts are presumably a consequence of RAPA's perturbation of the phospholipid bilayer. The RAPA's impact on the surface of DPPC-based anionic liposomes has been only recently elucidated [56], while the effect on the lipophilic moiety was studied earlier [57]. Table 2 shows the results of the differential scanning calorimetry (DSC) analysis, where the impact of RAPA on DPPC/DSPG liposomal bilayer was evaluated on unextruded liposomes (MLVs) and aggregated vesicles (ZnALs). High rigidity of the used unsaturated phospholipids limited the impact of the encapsulated drug on the bilayer's packing, as only a slight decrease in $T_m$ can be observed. A more significant effect is the widening of the transition peak, suggesting that the homogeneity of the bilayers is affected by RAPA. Expectedly, the pretransition peak at 36 °C disappeared in the drug-loaded sample (Table 2), suggestive of the drug's interaction with the polar headgroups or acyl chains of the phospholipids, as previously reported [56]. High Resolution Magic Angle Spinning (HR-MAS) NMR spectroscopic data obtained for RAPA-loaded liposomes did not yield the anticipated site-specific intermolecular interactions but offered a further proof of RAPA association with the liposomes based on spectral appearance and NOE results (Figure S3**a)–c)**). A greater effect of RAPA is observed in ZnALs, where both the transition and the pretransition peaks disappeared in the RAPA-loaded system, suggesting an altered packing of phospholipids. In summary, these DSC results show that RAPA affects the liposomal membrane, which could explain the differences in the aggregation behaviour in Fig. 2a**)** and **b)**.

Subsequently, the size and reversibility of ZnALs were determined by dilution with ultrapure water to below the minimal concentration of $Zn^{2+}$ that is needed for the aggregation (<0.5 mM). The 1.9 mM and 150 mM $Zn^{2+}$ concentrations were chosen for these measurements as they correspond to the first and second aggregation peaks respectively, which can be observed in Fig. 2a) and b). The measurements were performed with dynamic light scattering (DLS) and particle size analyser (PSA) that is based on laser diffraction technology, which is used to analyse particles in µm-range. The PSA measurements showed that the size distribution after 30 min of aggregation in 150 mM $Zn^{2+}$ and subsequent dilution was unimodal with the mean size of 96 µm ± 19 µm (Table 3 and Fig. 2**c**)), indicating that the aggregates are irreversible. Upon performing the same procedure with the ZnALs at 1.9 mM $Zn^{2+}$, the detector obscuration was found below 0.5 %, which points to deaggregation of ZnALs. Subsequent DLS measurement of the diluted samples revealed the reversion of ZnALs to the single-liposome size of 119 nm, which is the consequence of disaggregation. However, for ZnALs at 150 mM $Zn^{2+}$, the correlation function was irregular, and the size of aggregates could not be measured.

To confirm the presence of irreversible aggregates at 150 mM $Zn^{2+}$, a nanoparticle tracking analysis (NTA) was used to capture the ZnALs on video after they were diluted 400x in ultrapure water and can be seen in **Supplementary Video 1**. In contrast, no aggregates can be observed in **Supplementary Video 2**, where ZnALs with 1.9 mM $Zn^{2+}$ were diluted by the same dilution factor. The formation of irreversible aggregates was further studied by the addition of liposomes in excess volume of 150 mM $Zn^{2+}$ solution, while the liquid was continuously flowing through a flow cell that was in a closed loop of PSA instrument. Fig. 2**d)** shows the kinetic profile of size change for the period of 30 min. The aggregation reached its peak at 6 min of flowing through the flow cell at 122 µm and was followed by a decrease in size, which stabilised at 10 min. The gradual decrease in size over the following 20 min is likely due to shear stress, caused by the flow through the flow-cell. Taken together, these results demonstrate that ZnALs formed at 150 mM $Zn^{2+}$ concentration are irreversible, which distinguishes this system from previously studied reversible aggregates that were tested for for drug delivery purposes [32,33]. These studies did not achieve or test the global maximum in the aggregation profile of anionic liposomes within the explored cation concentrations. However, separate research on zwitterionic liposomes [58–60] examined the aggregation mechanism and the reversibility of liposomal aggregation. In this context, researchers linked the observed irreversible behaviour upon dilution with reaching the primary minimum, an observation that aligns with the DLVO theory of colloidal stability. The irreversibility of our system enables the removal of excess $Zn^{2+}$ through dialysis or tangential flow filtration, which was not possible in reversible systems. Our findings also show that the mean size of these aggregates is 96 µm, which exceeds the 10 µm threshold necessary for increased joint retention, as suggested by previous research [29,31]. The formation of irreversible aggregates not only adds value to our liposomal drug delivery system but also demonstrates the potential for enhanced joint retention in osteoarthritis treatment.

The morphology of liposomes and ZnALs were assessed with Cryo-TEM and the representative images are shown in Fig. 3. The liposomes were mainly unilamellar and nanosized, consistent with the DLS data. The empty liposomes occasionally flattened, wheras the addition of 1.9 mM $Zn^{2+}$, surprisingly, formed polyhedral structures with a negative curvature of the bilayer. Loaded liposomes only showed slight flattening at 1.9 mM and clear curvature at 150 mM $Zn^{2+}$ (Fig. 3 and **Supplementary Video 3**). This was not seen in our previous study with DPPC/

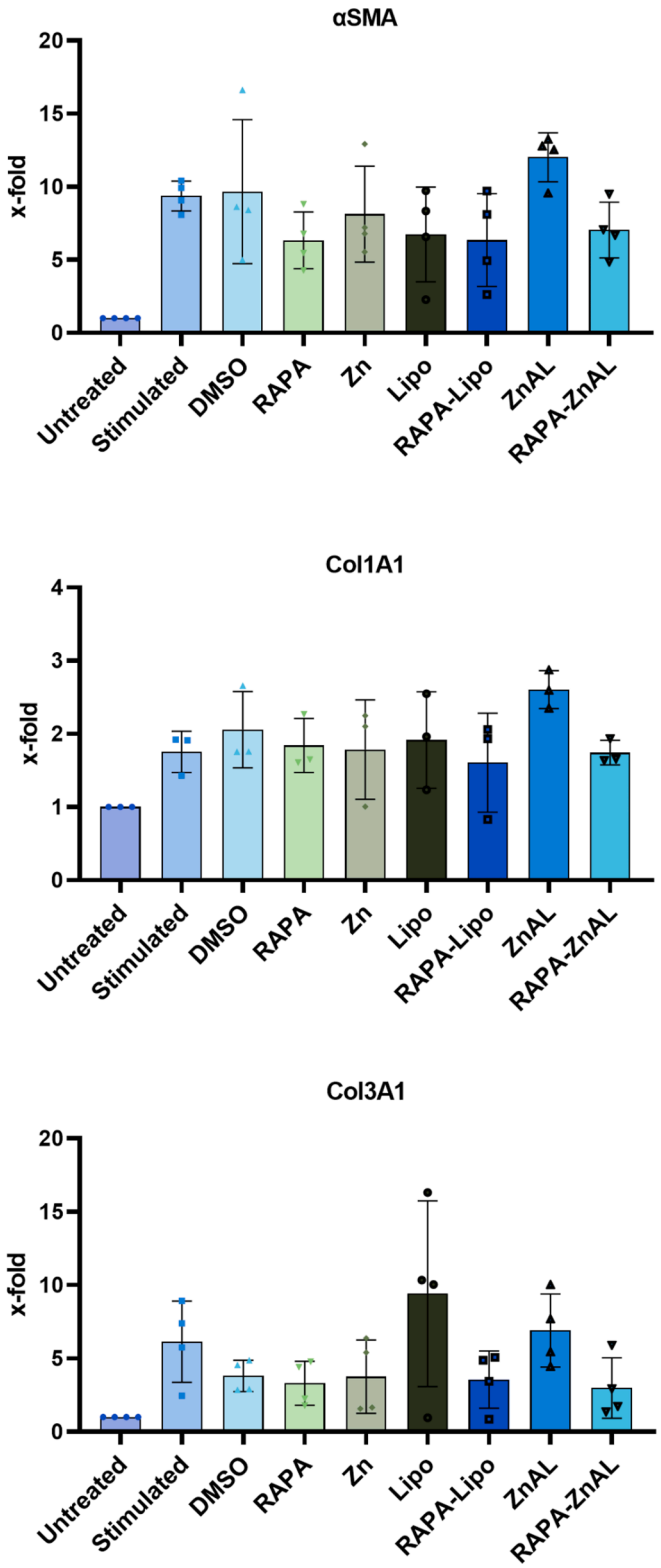


**Fig. 6.** Gene expression of a) αSMA, b) Col1A1, n) and Col3A1 in OASFs that were stimulated with TGFβ (10 ng/mL) and treated with specified conditions for 48 h.

DSPG/chol liposomes exposed to 10 mM divalent cation, where only aggregation was observed [33]. The obvious explanation for this is that the particles in the present study have an enhanced fluid character due to the lack of chol in the bilayer and the formation of polyhedral structures is energetically favourable under the osmotic pressure imposed by external $Zn^{2+}$. It has been previously reported that nano-sized rigid liposomes can exist in a facetted configuration below their $T_m$ [61]. The fact that RAPA-loaded liposomes exhibit a reduced angularity in up to 20 mM $Zn^{2+}$ concentration suggests that the encapsulation of the drug in the bilayer has a chol-like effect on the membrane. This increased fluidity of the membrane is also supported by the DSC results in Table 2. The stabilization of liposomes' spherical morphology by hydrophobic molecules is further supported by earlier investigation of the temoporfin encapsulation, which has comparable solubility in water to RAPA and has similarly reduced the angularity of the particles [62]. These results not only have importance for the design of liposomal drug delivery systems, but have further implications for better understanding of the cell membrane dynamics in different tonicities, as living cells also contain hydrophobic solutes. Furthermore, cryoTEM (Fig. 3) confirmed the presence of aggregates at 1.9 mM and 150 mM $Zn^{2+}$, which corroborated the PSA results.

Empty liposomes had clear aggregation at 20 mM $Zn^{2+}$, while RAPA-loaded samples showed less pronounced aggregation as seen in Fig. 2a). Large aggregates were also scanned three-dimensionally using cryo-TEM tomography and are presented in **Supplementary Video 3**. To observe the system at a larger scale, liposomes were fluorescently labelled with DiD and aggregated as before (*vide supra*). **Figure S5** shows complex morphology of large ZnALs at 150 mM $Zn^{2+}$. While our imaging techniques have provided key insights into the liposomal aggregates, future studies could further explore their interaction with cartilage. Techniques such as confocal Raman microscopy could elucidate the aggregates' spatial distribution within cartilage, while AFM measurements could provide insights into surface roughness, and phospholipid layer rigidity, which could have implications for the tribological behaviour of the system.

### 3.3. RAPA release from ZnALs and effect on human OASFs

RAPA release from liposomes and ZnALs was tested in 10% EtOH in water to ensure sink conditions and stability of the drug throughout the experiment. Fig. 4a) shows that ZnALs could retain the drug for longer than free liposomes with 86% released after 7 days, while 90% of the cargo was released from free liposomes already after 3 days. This difference in release rate can be attributed to the distinct diffusion pathways in aggregated and non-aggregated liposomes. In aggregated liposomes, the drug must navigate through multiple barriers consisting of interconnected phospholipid bilayers, thereby leading to a more prolonged release process. Conversely, non-aggregated liposomes offer a simpler release mechanism, wherein the drug traverses a single membrane of the small unilamellar vesicle, resulting in an accelerated release rate. The difference in the release rates of bupivacaine from aggregated DSPG liposomes and plain liposomes was previously described by our group and confirmed *in vivo* with the pharmacokinetic study [33]. The use of aggregated liposomes for sustained drug delivery was recently proposed by our group in a study, where bupivacaine's release was retained *in vitro* by calcium aggregated liposomes and the bioavailability of the drug was increased *in vivo* [33].

However, the previously reported aggregates needed an outside source of cations to retain the aggregated state and control the drug release. In our study, however, ZnALs were shown to be irreversible and exhibited a prolonged release even without the addition of $Zn^{2+}$ in the release medium. These results suggest that ZnALs could potentially decrease the need for frequent intraarticular administration, which was previously connected with an increased risk of infections [28]. RAPA did not induce any toxicity in human OASFs after 48 h incubation with the drug in the range of 5 ng/mL up to 10 μg/mL, as reported in Fig. 4**b-e)**. Next, the cells were stimulated with transforming growth factor-beta (TGFβ), a key mediator of synovial fibrosis in OA, to induce disease-like fibrotic response [2,16,17]. Fig. 4**f)** and **g)** show that 1 μg/mL RAPA was able to decrease the gene expression of key profibrotic markers, in the OASFs, namely αSMA and Col1A1. Previous studies

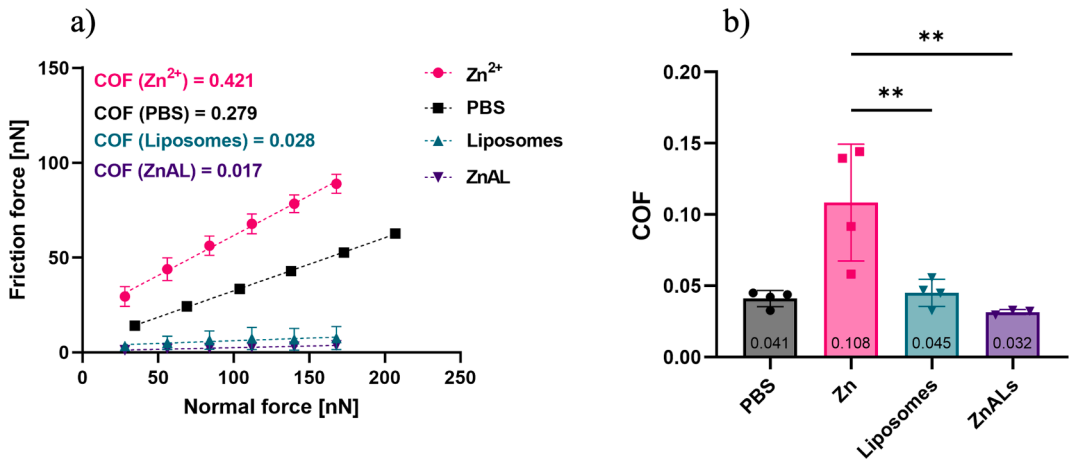


**Fig. 7.** a) Friction as measured with CP-LFM on silicon substrate. b) Friction as measured with UMT on ex vivo porcine cartilage. ZnALs were purified before testing as described above. One-way ANOVA with Tukey's multiple comparisons test was run. statistical significance is designated as: *p < 0.05 **P < 0.01, ***P < 0.001, ****P < 0.0001. In all tests, liposomes and ZnAL had a total lipid concentration of 5 mM, while 23 mM was the final $Zn^{2+}$ concentration in ZnALs after dialysis and in $Zn^{2+}$ condition.

reported that RAPA can decrease inflammation and chondrocyte senescence in the synovial joints [12,14,63]. Our results add to this by showing that RAPA dampens fibrotic signaling in human OASFs *in vitro*. Furthermore, the toxicity of $Zn^{2+}$ and RAPA in ZnALs was tested to find the dose for gene expression experiments. ZnALs were purified with dialysis prior to testing and the final $Zn^{2+}$ concentration was measured with ICP-MS. RAPA content in purified ZnALs with 0.5 mM $Zn^{2+}$ was 100 ng/mL and the ratio between the two was kept constant for higher doses (**Table S1**). No significant toxicity was observed at 0.5 mM of $Zn^{2+}$, while 5 mM induced cell death (Fig. 5).

The same $Zn^{2+}$ concentration is present in purified ZnALs with 1 μg/mL RAPA content (**Table S1**), where a similar toxic effect was observed. For these reasons, purified ZnALs with 100 ng/mL dose of RAPA were used for further cell experiments. The gene expression data in Fig. 6a**)–c)** show that 100 ng/mL RAPA did not decrease fibrotic markers as effectively as 1 μg/mL. This calls for further research to find a more potent drug or a less toxic aggregating agent.

### 3.4. Lubrication of cartilage

Lubrication properties of the system were analysed with colloidal probe lateral force microscopy (CP-LFM) on silicon surface and a UMT-2 macro-tribometer with self-mated *ex vivo* porcine cartilage. The silicon used as a substrate for CP-LFM measurement was thoroughly cleaned to ensure a negative surface charge, in order to mimic the chemistry of the cartilage surface. Fig. 7a**)** shows the change in friction force as the applied normal force is increased for the silicon surfaces treated with different conditions, as previously described [22]. The measured friction coefficient (COF) values obtained from the slope of the curve, drastically decreased when the surface was treated with liposomes and purified ZnALs (0.017) in comparison to PBS (0.279). It is generally accepted that the superior lubrication of liposomes stems from the formation of a hydration shell around the dipole of phospholipids, which can support high compressive loads and is very fluid [24,64]. A similar mechanism is expected here after the treatment with ZnALs, whose mean COF is lower compared to the liposomes', which is 0.028. While hydration is also anticipated in the case of $Zn^{2+}$ treatment, the results demonstrate a significant increase in friction (0.421). The plot of normal force versus friction force (Fig. 7a)) for silica sliding against silicon submerged in a $Zn^{2+}$ solution does not pass through zero, indicating a substantial adhesive component. This can be attributed to the positively charged $Zn^{2+}$ surface interacting with the negatively charged silica countersurface. This observation suggests that the hydration shell formed around the zinc ions is not sufficient to counterbalance the adhesive forces between the probe and the $Zn^{2+}$-coated silica surface, increasing the COF.

A similar trend can be observed Fig. 7b**)**, where the COF was measured on *ex vivo* cartilage with a macro-tribometer. The presence of zinc ions drastically increased the friction on the cartilage to a COF of 0.108 compared to the PBS of 0.041. $Zn^{2+}$ is classed as strongly kosmotropic and may be influencing the aggregation of proteins and their hydration within the cartilage. As the mechanical and tribological behaviour of cartilage is strongly dependant on hydration, a change is expected to have an influence on the friction properties. Ionic kosmotropes tend to reduce the diffusion of water and separate into more dense water. This increase by the metal cations was negated by the electrostatic adsorption on the negatively charged liposomes and the formation of ZnALs, which significantly decreased the COF to 0.032. It is proposed that the liposomes hold the $Zn^{2+}$ at the surface, thus reducing its influence on the bulk cartilage and forming a protective coating on the surface. The mean COF of the free liposomes was measured at 0.045. To our knowledge, this is the first tribological study of liposomal aggregates. Taken together, the formation of aggregates improved the friction on nano-tribological scale and protected cartilage on macro-tribological scale, which indicates the potential of the formulation for the treatment of damaged cartilage in OA. More research is needed to confirm the observed responses under physiological conditions and determine the influence of liposomes and ZnALs on wear.

## 4. Conclusion

In the present report, we show that the aggregation of negatively charged liposomes with 150 mM $Zn^{2+}$ yields irreversible aggregates (ZnALs) with a diameter above 90 μm, which was reported to drastically increase retention in synovial joints. We characterised the aggregation properties in depth and showed that ZnALs can sustain the release of RAPA, which decreases fibrotic markers in human OASFs. While necessary for the aggregation and the controlled release, $Zn^{2+}$'s toxicity limits the therapeutic window of ZnALs. Aggregate formation prevents the increase of friction due to the presence of $Zn^{2+}$ *ex vivo*, significantly decreasing the friction coefficient (COF) to 0.032, below the PBS control. The same effect was observed in a nanotribological setting, where ZnALs lowered the COF compared with free zinc ions and outperformed PBS. In summary, ZnALs are a drug delivery system that can sustain the release of RAPA longer than free liposomes, with 86 % of the drug released at 7-day mark. Future research should focus on improvements in the toxicity profile of the aggregated liposomes by finding new aggregating agents and thus improving the therapeutic effect of the formulation.

## CRediT authorship contribution statement

**Gregor Bordon:** Conceptualization, Funding acquisition, Investigation, Validation, Visualization, Formal analysis, Data curation, Writing – original draft. **Shivaprakash N. Ramakrishna:** Methodology, Investigation. **Sam G. Edalat:** Methodology. **Remo Eugster:** Investigation, Validation. **Andrea Arcifa:** Methodology. **Martina Vermathen:** Methodology, Investigation, Visualization. **Simone Aleandri:** Methodology. **Mojca Frank Bertoncelj:** Conceptualization, Supervision. **Julien Furrer:** Funding acquisition, Supervision. **Peter Vermathen:** Funding acquisition, Supervision. **Lucio Isa:** Funding acquisition. **Rowena Crockett:** Funding acquisition, Supervision. **Oliver Distler:** Funding acquisition, Supervision. **Paola Luciani:** Conceptualization, Supervision, Project administration, Funding acquisition.

## Declaration of Competing Interest

The authors declare the following financial interests/personal relationships which may be considered as potential competing interests: OD has/had consultancy relationship with and/or has received research funding from and/or has served as a speaker for the following companies in the last three calendar years: 4P-Pharma, Abbvie, Acceleron, Alcimed, Altavant, Amgen, AnaMar, Arxx, AstraZeneca, Blade, Bayer, Boehringer Ingelheim, Corbus, CSL Behring, Galderma, Galapagos, Glenmark, Gossamer, Horizon, Janssen, Kymera, Lupin, Medscape, Merck, Miltenyi Biotec, Mitsubishi Tanabe, Novartis, Pfizer, Prometheus, Redxpharma, Roivant and Topadur. **Patent** issued "mir-29 for the treatment of systemic sclerosis" (US8247389, EP2331143). PL has consulted and received research funding from Lipoid GmbH, Sanofi-Aventis Deutschland and DSM Nutritional Products Ltd.

## Data availability

Data will be made available on request.

## Acknowledgments

This work was supported by The Open Round grant by the Faculty of Science of the University of Bern. The authors thank the Center for Microscopy and Image Analysis at the University of Zurich for maintaining the imaging equipment and Dr. Elena Pachera for her support in acquiring images, as well as Peter Künzler and Benvinda Henriques Campos for their valuable support in the cell culture laboratories. Aggregation kinetics and aggregates' size were measured and analysed with the kind support of Anton Paar TriTec SA in Neuchâtel. Fresh preparation of liposomes for cell experiments was possible thanks to the hospitality of Prof. Jean-Christoph Leroux and his team at ETH Zürich. The authors are grateful to Nicola Lüdi at Department of Chemistry, Biochemistry and Pharmaceutical Sciences of the University of Bern for his support with ICP-MS measurements. The authors would also like to thank the workshop of Department of Chemistry, Biochemistry and Pharmaceutical Sciences of the University of Bern for making the dialysis devices for *in vitro* drug release experiments. Frank Steiniger of the University of Jena, Germany, is warmly acknowledged for his support with the cryo-TEM image acquisition and analysis of RAPA-loaded liposomes.

## Appendix A. Supplementary material

Supplementary data to this article can be found online at https://doi.org/10.1016/j.jcis.2023.07.087.

## References

[1] I.A. Jones, R. Togashi, M.L. Wilson, N. Heckmann, C.T. Vangsness, Intra-articular treatment options for knee osteoarthritis, Nat. Rev. Rheumatol. 15 (2018) 77–90, https://doi.org/10.1038/s41584-018-0123-4.

[2] A. Maglaviceanu, B. Wu, M. Kapoor, Fibroblast-like synoviocytes: Role in synovial fibrosis associated with osteoarthritis, Wound Repair Regen. 29 (2021) 642–649, https://doi.org/10.1111/WRR.12939.

[3] D.J. Hunter, L. March, M. Chew, Osteoarthritis in 2020 and beyond: a Lancet Commission, Lancet. 396 (2020) 1711–1712, https://doi.org/10.1016/S0140-6736(20)32230-3.

[4] J. Camardo, T. Rapamune, era of immunosuppression,, the journey from the laboratory to clinical transplantation, Transplant. Proc. 35 (2003) (2003) S18–S24, https://doi.org/10.1016/S0041-1345(03)00356-7.

[5] L.H. Meng, X.S. Zheng, Toward rapamycin analog (rapalog)-based precision cancer therapy, Acta Pharmacol. Sin. 36 (2015) 1163–1169, https://doi.org/10.1038/aps.2015.68.

[6] W. Wu, Z. He, Z. Zhang, X. Yu, Z. Song, X. Li, Intravitreal injection of rapamycin-loaded polymeric micelles for inhibition of ocular inflammation in rat model, Int. J. Pharm. 513 (2016) 238–246, https://doi.org/10.1016/j.ijpharm.2016.09.013.

[7] S. Chen, M.N. van Tok, V.L. Knaup, L. Kraal, D. Pots, L. Bartels, E.M. Gravallese, J. D. Taurog, M. van de Sande, L.M. van Duivenvoorde, D.L. Baeten, mTOR Blockade by Rapamycin in Spondyloarthritis: Impact on Inflammation and New Bone Formation in vitro and in vivo, Front. Immunol. 10 (2020) 2344, https://doi.org/10.3389/FIMMU.2019.02344.

[8] Z.W. Lai, R. Kelly, T. Winans, I. Marchena, A. Shadakshari, J. Yu, M. Dawood, R. Garcia, H. Tily, L. Francis, S.V. Faraone, P.E. Phillips, A. Perl, Sirolimus in patients with clinically active systemic lupus erythematosus resistant to, or intolerant of, conventional medications: a single-arm, open-label, phase 1/2 trial, Lancet. 391 (2018) 1186–1196, https://doi.org/10.1016/S0140-6736(18)30485-9.

[9] T. Weichhart, mTOR as Regulator of Lifespan, Aging, and Cellular Senescence: A Mini-Review, Gerontology. 64 (2018) 127–134, https://doi.org/10.1159/000484629.

[10] J.E. Wilkinson, L. Burmeister, S.V. Brooks, C.C. Chan, S. Friedline, D.E. Harrison, J. F. Hejtmancik, N. Nadon, R. Strong, L.K. Wood, M.A. Woodward, R.A. Miller, Rapamycin slows aging in mice, Aging Cell. 11 (2012) 675–682, https://doi.org/10.1111/J.1474-9726.2012.00832.X.

[11] A. Perl, Activation of mTOR (mechanistic target of rapamycin) in rheumatic diseases, Nat. Rev. Rheumatol. 12 (2015) 169–182, https://doi.org/10.1038/nrrheum.2015.172.

[12] H. Sasaki, K. Takayama, T. Matsushita, K. Ishida, S. Kubo, T. Matsumoto, N. Fujita, S. Oka, M. Kurosaka, R. Kuroda, Autophagy modulates osteoarthritis-related gene expression in human chondrocytes, Arthritis Rheum. 64 (2012) 1920–1928, https://doi.org/10.1002/ART.34323.

[13] K. Takayama, Y. Kawakami, M. Kobayashi, N. Greco, J.H. Cummins, T. Matsushita, R. Kuroda, M. Kurosaka, F.H. Fu, J. Huard, Local intra-articular injection of rapamycin delays articular cartilage degeneration in a murine model of osteoarthritis, Arthritis Res. Ther. 16 (2014) 1–10, https://doi.org/10.1186/S13075-014-0482-4.

[14] T. Matsuzaki, T. Matsushita, Y. Tabata, T. Saito, T. Matsumoto, K. Nagai, R. Kuroda, M. Kurosaka, Intra-articular administration of gelatin hydrogels incorporating rapamycin–micelles reduces the development of experimental osteoarthritis in a murine model, Biomaterials 35 (2014) 9904–9911, https://doi.org/10.1016/J.BIOMATERIALS.2014.08.041.

[15] B. Caramés, A. Hasegawa, N. Taniguchi, S. Miyaki, F.J. Blanco, M. Lotz, Autophagy activation by rapamycin reduces severity of experimental osteoarthritis, Ann. Rheum. Dis. 71 (2012) 575, https://doi.org/10.1136/ANNRHEUMDIS-2011-200557.

[16] Y. Zhang, F. Vasheghani, Y.H. Li, M. Blati, K. Simeone, H. Fahmi, B. Lussier, P. Roughley, D. Lagares, J.P. Pelletier, J. Martel-Pelletier, M. Kapoor, Cartilage-specific deletion of mTOR upregulates autophagy and protects mice from osteoarthritis, Ann. Rheum. Dis. 74 (2015) 1432–1440, https://doi.org/10.1136/ANNRHEUMDIS-2013-204599.

[17] J. Shen, S. Li, D. Chen, TGF-β signaling and the development of osteoarthritis, Bone Res. 2 (2014) 1–7, https://doi.org/10.1038/boneres.2014.2.

[18] J. Friščić, M. Böttcher, C. Reinwald, H. Bruns, B. Wirth, S.J. Popp, K.I. Walker, J. A. Ackermann, X. Chen, J. Turner, H. Zhu, L. Seyler, M. Euler, P. Kirchner, R. Krüger, A.B. Ekici, T. Major, O. Aust, D. Weidner, A. Fischer, F.T. Andes, Z. Stanojevic, V. Trajkovic, M. Herrmann, A. Korb-Pap, I. Wank, A. Hess, J. Winter, V. Wixler, J. Distler, G. Steiner, H.P. Kiener, B. Frey, L. Kling, K. Raza, S. Frey, A. Kleyer, T. Bäuerle, T.R. Hughes, A. Grüneboom, U. Steffen, G. Krönke, A. P. Croft, A. Filer, J. Köhl, K. Klein, C.D. Buckley, G. Schett, D. Mougiakakos, M. H. Hoffmann, The complement system drives local inflammatory tissue priming by metabolic reprogramming of synovial fibroblasts, Immunity 54 (2021) 1002–1021.e10, https://doi.org/10.1016/J.IMMUNI.2021.03.003.

[19] W.C. Chen, S.W. Wang, C.Y. Lin, C.H. Tsai, Y.C. Fong, T.Y. Lin, S.L. Weng, H. Da Huang, K.W. Liao, C.H. Tang, Resistin enhances monocyte chemoattractant protein-1 production in human synovial fibroblasts and facilitates monocyte migration, Cell. Physiol. Biochem. 52 (2019) 408–420, https://doi.org/10.33594/000000029.

[20] T. Karonitsch, R.K. Kandasamy, F. Kartnig, B. Herdy, K. Dalwigk, B. Niederreiter, J. Holinka, F. Sevelda, R. Windhager, M. Bilban, T. Weichhart, M. Säemann, T. Pap, G. Steiner, J.S. Smolen, H.P. Kiener, G. Superti-Furga, mTOR senses environmental cues to shape the fibroblast-like synoviocyte response to inflammation, Cell Rep. 23 (2018) 2157–2167, https://doi.org/10.1016/J.CELREP.2018.04.044.

[21] Y. Lei, Y. Wang, J. Shen, Z. Cai, C. Zhao, H. Chen, X. Luo, N. Hu, W. Cui, W. Huang, Injectable hydrogel microspheres with self-renewable hydration layers alleviate osteoarthritis, Sci. Adv. 8 (2022), https://doi.org/10.1126/SCIADV.ABL6449.
[22] X. Ji, Y. Yan, T. Sun, Q. Zhang, Y. Wang, M. Zhang, H. Zhang, X. Zhao, Glucosamine sulphate-loaded distearoyl phosphocholine liposomes for osteoarthritis treatment: combination of sustained drug release and improved lubrication, Biomater. Sci. 7 (2019) 2716–2728, https://doi.org/10.1039/C9BM00201D.
[23] B.A. Hills, B.D. Butler, Surfactants identified in synovial fluid and their ability to act as boundary lubricants, Ann. Rheum. Dis. 43 (1984) 641–648, https://doi.org/10.1136/ard.43.4.641.
[24] W. Lin, J. Klein, W. Lin, J. Klein, Recent progress in cartilage lubrication, Adv. Mater. 33 (2021) 2005513, https://doi.org/10.1002/ADMA.202005513.
[25] R. Goldberg, J. Klein, Liposomes as lubricants: beyond drug delivery, Chem. Phys. Lipids. 165 (2012) 374–381, https://doi.org/10.1016/J.CHEMPHYSLIP.2011.11.007.
[26] G. Verberne, A. Schroeder, G. Halperin, Y. Barenholz, I. Etsion, Liposomes as potential biolubricant additives for wear reduction in human synovial joints, Wear. 268 (2010) 1037–1042, https://doi.org/10.1016/J.WEAR.2009.12.037.
[27] S. Sivan, A. Schroeder, G. Verberne, Y. Merkher, D. Diminsky, A. Priev, A. Maroudas, G. Halperin, D. Nitzan, I. Etsion, Y. Barenholz, Liposomes act as effective biolubricants for friction reduction in human synovial joints, Langmuir. 26 (2010) 1107–1116, https://doi.org/10.1021/LA9024712.
[28] C. Albert, O. Brocq, D. Gerard, C. Roux, L. Euller-Ziegler, Septic knee arthritis after intra-articular hyaluronate injection: Two case reports, Jt. Bone Spine. 73 (2006) 205–207, https://doi.org/10.1016/J.JBSPIN.2005.03.005.
[29] J. Pradal, P. Maudens, C. Gabay, C.A. Seemayer, O. Jordan, E. Allémann, Effect of particle size on the biodistribution of nano- and microparticles following intra-articular injection in mice, Int. J. Pharm. 498 (2016) 119–129, https://doi.org/10.1016/J.IJPHARM.2015.12.015.
[30] J. Dong, D. Jiang, Z. Wang, G. Wu, L. Miao, L. Huang, Intra-articular delivery of liposomal celecoxib–hyaluronate combination for the treatment of osteoarthritis in rabbit model, Int. J. Pharm. 441 (2013) 285–290, https://doi.org/10.1016/J.IJPHARM.2012.11.031.
[31] J.A. Champion, A. Walker, S. Mitragotri, Role of particle size in phagocytosis of polymeric microspheres, Pharm. Res. 25 (2008) 1815–1821, https://doi.org/10.1007/S11095-008-9562-Y.
[32] L. Rahnfeld, J. Thamm, F. Steiniger, P. van Hoogevest, P. Luciani, Study on the in situ aggregation of liposomes with negatively charged phospholipids for use as injectable depot formulation, Colloids Surf. B Biointerf. 168 (2018) 10–17, https://doi.org/10.1016/j.colsurfb.2018.02.023.
[33] S. Aleandri, L. Rahnfeld, D. Chatzikleanthous, A. Bergadano, C. Bühr, C. Detotto, S. Fuochi, K. Weber-Wilk, S. Schürch, P. van Hoogevest, P. Luciani, Development and in vivo validation of phospholipid-based depots for the sustained release of bupivacaine, Eur. J. Pharm. Biopharm. 181 (2022) 300–309, https://doi.org/10.1016/j.ejpb.2022.11.019.
[34] A.S. Prasad, Clinical, immunological, anti-inflammatory and antioxidant roles of zinc, Exp. Gerontol. 43 (2008) 370–377, https://doi.org/10.1016/J.EXGER.2007.10.013.
[35] A.S. Prasad, Zinc is an antioxidant and anti-inflammatory agent: Its role in human health, Front. Nutr. 1 (2014) 14, https://doi.org/10.3389/FNUT.2014.00014.
[36] M. Jarosz, M. Olbert, G. Wyszogrodzka, K. Młyniec, T. Librowski, Antioxidant and anti-inflammatory effects of zinc. Zinc-dependent NF-κB signaling, Inflammopharmacology 25 (2017) 11–24, https://doi.org/10.1007/S10787-017-0309-4.
[37] M. Ricciutelli, P. Di Martino, L. Barboni, S. Martelli, Evaluation of rapamycin chemical stability in volatile-organic solvents by HPLC, J. Pharm. Biomed. Anal. 41 (2006) 1070–1074, https://doi.org/10.1016/J.JPBA.2006.02.009.
[38] F. Alexis, S.S. Venkatraman, S.K. Rath, F. Boey, In vitro study of release mechanisms of paclitaxel and rapamycin from drug-incorporated biodegradable stent matrices, J. Control. Release. 98 (2004) 67–74, https://doi.org/10.1016/J.JCONREL.2004.04.011.
[39] X. Ge, M. Frank-Bertoncelj, K. Klein, A. McGovern, T. Kuret, M. Houtman, B. Burja, R. Micheroli, C. Shi, M. Marks, A. Filer, C.D. Buckley, G. Orozco, O. Distler, A. P. Morris, P. Martin, S. Eyre, C. Ospelt, Functional genomics atlas of synovial fibroblasts defining rheumatoid arthritis heritability, Genome Biol. 22 (2021) 1–39, https://doi.org/10.1186/S13059-021-02460-6.
[40] T.D. Schmittgen, E.J. Lee, J. Jiang, A. Sarkar, L. Yang, T.S. Elton, C. Chen, Real-time PCR quantification of precursor and mature microRNA, Methods 44 (2008) 31–38, https://doi.org/10.1016/J.YMETH.2007.09.006.
[41] J.L. Hutter, J. Bechhoefer, Calibration of atomic-force microscope tips, Rev. Sci. Instrum. 64 (1998) 1868, https://doi.org/10.1063/1.1143970.
[42] C.P. Green, H. Lioe, J.P. Cleveland, R. Proksch, P. Mulvaney, J.E. Sader, Normal and torsional spring constants of atomic force microscope cantilevers, Rev. Sci. Instrum. 75 (2004) 1988, https://doi.org/10.1063/1.1753100.
[43] R.J. Cannara, M. Eglin, R.W. Carpick, Lateral force calibration in atomic force microscopy: A new lateral force calibration method and general guidelines for optimization, Rev. Sci. Instrum. 77 (2006), 053701, https://doi.org/10.1063/1.2198768.
[44] J. Gubernator, Active methods of drug loading into liposomes: recent strategies for stable drug entrapment and increased in vivo activity, Expert Opin. Drug Deliv. 8 (2011) 565–580, https://doi.org/10.1517/17425247.2011.566552.
[45] M. Chountoulesi, N. Naziris, N. Pippa, C. Demetzos, The significance of drug-to-lipid ratio to the development of optimized liposomal formulation, J. Liposome Res. 28 (2017) 249–258, https://doi.org/10.1080/08982104.2017.1343836.
[46] A. Haeri, S. Sadeghian, S. Rabbani, M.S. Anvari, M.A. Boroumand, S. Dadashzadeh, Use of remote film loading methodology to entrap sirolimus into liposomes: Preparation, characterization and in vivo efficacy for treatment of restenosis, Int. J. Pharm. 414 (2011) 16–27, https://doi.org/10.1016/j.ijpharm.2011.04.055.
[47] M.A. Rouf, I. Vural, J.M. Renoir, A.A. Hincal, Development and characterization of liposomal formulations for rapamycin delivery and investigation of their antiproliferative effect on MCF7 cells, J. Liposome Res. 19 (2009) 322–331, https://doi.org/10.3109/08982100902963043.
[48] B. Sylvester, A. Porfire, D.M. Muntean, L. Vlase, L. Lupuţ, E. Licarete, A. Sesarman, M.C. Alupei, M. Banciu, M. Achim, I. Tomuţă, Optimization of prednisolone-loaded long-circulating liposomes via application of Quality by Design (QbD) approach, J. Liposome Res. 28 (2016) 49–61, https://doi.org/10.1080/08982104.2016.1254242.
[49] J.A. Zhang, G. Anyarambhatla, L. Ma, S. Ugwu, T. Xuan, T. Sardone, I. Ahmad, Development and characterization of a novel Cremophor® EL free liposome-based paclitaxel (LEP-ETU) formulation, Eur. J. Pharm. Biopharm. 59 (2005) 177–187, https://doi.org/10.1016/J.EJPB.2004.06.009.
[50] F. Lin, Z. Wang, L. Xiang, L. Deng, W. Cui, F. Lin, Z. Wang, L. Xiang, L. Deng, W. Cui, Charge-guided micro/nano-hydrogel microsphere for penetrating cartilage matrix, Adv. Funct. Mater. 31 (2021) 2107678, https://doi.org/10.1002/ADFM.202107678.
[51] X.L. Xu, Y. Xue, J.Y. Ding, Z.H. Zhu, X.C. Wu, Y.J. Song, Y.L. Cao, L.G. Tang, D. F. Ding, J.G. Xu, Nanodevices for deep cartilage penetration, Acta Biomater. 154 (2022) 23–48, https://doi.org/10.1016/J.ACTBIO.2022.10.007.
[52] C.T. Inglut, A.J. Sorrin, T. Kuruppu, S. Vig, J. Cicalo, H. Ahmad, H.C. Huang, Immunological and toxicological considerations for the design of liposomes, Nanomater. 10 (2020) 190, https://doi.org/10.3390/NANO10020190.
[53] M.C. Filion, N.C. Phillips, Toxicity and immunomodulatory activity of liposomal vectors formulated with cationic lipids toward immune effector cells, Biochim. Biophys. Acta - Biomembr. 1329 (1997) 345–356, https://doi.org/10.1016/S0005-2736(97)00126-0.
[54] D. Volodkin, V. Ball, P. Schaaf, J.C. Voegel, H. Mohwald, Complexation of phosphocholine liposomes with polylysine. Stabilization by surface coverage versus aggregation, Biochim. Biophys. Acta - Biomembr. 1768 (2007) 280–290, https://doi.org/10.1016/J.BBAMEM.2006.09.015.
[55] A. Gorman, K.R. Hossain, F. Cornelius, R.J. Clarke, Penetration of phospholipid membranes by poly-l-lysine depends on cholesterol and phospholipid composition, Biochim. Biophys. Acta - Biomembr. 1862 (2020), 183128, https://doi.org/10.1016/J.BBAMEM.2019.183128.
[56] I.M. Le-Deygen, A.S. Safronova, P.V. Mamaeva, I.M. Kolmogorov, A.A. Skuredina, E.V. Kudryashova, Drug–membrane interaction as revealed by spectroscopic methods: The role of drug structure in the example of rifampicin, Levofloxacin and Rapamycin, Biophys. 2 (2022) 353–365, https://doi.org/10.3390/BIOPHYSICA2040032.
[57] I. Onyesom, D.A. Lamprou, L. Sygellou, S.K. Owusu-Ware, M. Antonijevic, B. Z. Chowdhry, D. Douroumis, Sirolimus encapsulated liposomes for cancer therapy: Physicochemical and mechanical characterization of sirolimus distribution within liposome bilayers, Mol. Pharm. 10 (2013) 4281–4293, https://doi.org/10.1021/MP400362V.
[58] J. Sabín, G. Prieto, J.M. Ruso, F. Sarmiento, Fractal aggregates induced by liposome-liposome interaction in the presence of Ca2+, Eur. Phys. J. E 24 (2007) 201–210, https://doi.org/10.1140/EPJE/I2007-10231-3.
[59] J. Sabín, G. Prieto, J.M. Ruso, P. Messina, F. Sarmiento, Aggregation of liposomes in presence of La3+: A study of the fractal dimension, Phys. Rev. E - Stat. Nonlinear, Soft Matter Phys. 76 (2007), 011408, https://doi.org/10.1103/PHYSREVE.76.011408.
[60] J. Sabín, G. Prieto, F. Sarmiento, Stable clusters in liposomic systems, Soft Matter. 8 (2012) 3212–3222, https://doi.org/10.1039/C2SM06907E.
[61] E. Freire, C.F. Schmidt, P.L. Feigner, T.E. Thompson, D. Lichtenberg, Y. Barenholz, Effect of surface curvature on stability, thermodynamic behavior, and osmotic activity of dipalmitoylphosphatidylcholine single lamellar vesicles, Biochemistry 20 (1981) 3462–3467, https://doi.org/10.1021/BI00515A024.
[62] J. Kuntsche, I. Freisleben, F. Steiniger, A. Fahr, Temoporfin-loaded liposomes: Physicochemical characterization, Eur. J. Pharm. Sci. 40 (2010) 305–315, https://doi.org/10.1016/J.EJPS.2010.04.005.
[63] K.M. Dhanabalan, V.K. Gupta, R. Agarwal, Rapamycin–PLGA microparticles prevent senescence, sustain cartilage matrix production under stress and exhibit prolonged retention in mouse joints, Biomater. Sci. 8 (2020) 4308–4321, https://doi.org/10.1039/D0BM00596G.
[64] A. Gaisinskaya-Kipnis, J. Klein, Normal and frictional interactions between liposome-bearing biomacromolecular bilayers, Biomacromolecules. 17 (2016) 2591–2602, https://doi.org/10.1021/ACS.BIOMAC.6B00614.